Investigation of the compound $Hf_2Ni$: the electronic structure and the electric field gradient



1998 J. Phys.: Condens. Matter 10 6285

(http://iopscience.iop.org/0953-8984/10/28/010)

J. Phys.: Condens. Matter **10** (1998) 6285–6299. Printed in the UK PII: S0953-8984(98)90840-2

# Investigation of the compound $Hf_2Ni$: the electronic structure and the electric field gradient

M V Lalić, B Cekić, Z S Popović and F R Vukajlović
'Vinča' Institute of Nuclear Sciences, PO Box 522, 11001 Belgrade, Yugoslavia

Received 19 January 1998, in final form 8 April 1998

**Abstract.** The electronic structure and electric field gradient (EFG) of the intermetallic compound $Hf_2Ni$ are calculated on the basis of a recently developed first-principles band-structure full-potential (FP) linear-muffin-tin-orbital (LMTO) scheme within the atomic sphere approximation (ASA). The calculated value of the EFG at the Hf sites is in very good agreement with the results obtained by the time-differential perturbed angular correlation (TDPAC) technique used for the experimental study of the EFG at $^{181}$Ta impurity sites in the compound $Hf_2Ni$. The asymmetry parameter $\eta$ and the individual contributions to the EFG are discussed. It is shown that various treatments of 4f hafnium electrons have a large influence on the EFG. The formulae for all of the components of the EFG tensor (the contributions from the valence electrons as well as the lattice contribution) are derived and presented also.

## 1. Introduction

The quantities relevant for hyperfine interactions, like the electric field gradient (EFG) tensor and the isomer shift arising from the electron density at a specific nucleus, have been widely investigated recently both experimentally and theoretically. In order to obtain information about local chemical bonding characteristics, we need to understand the behaviour of the EFG and require a good account of the electronic structural properties of the compounds investigated. The direct relation of the EFG and the asphericity of the electron density in the vicinity of the probe nucleus enables one to estimate, from the quadrupole splitting, the degree of covalency or ionicity of chemical bonds in solids if the nuclear quadrupole moment is known.

The interaction between the nuclear quadrupole moment and the electric field gradient at an atomic site with non-cubic point symmetry can be determined by means of various hyperfine interaction measurements, such as time-differential perturbed angular correlation (TDPAC), perturbed angular correlation (PAC), and nuclear magnetic resonance (NMR) measurements. These methods have been used widely to obtain information about impurities, surfaces, and vacancy-related defects [1–8].

In contrast to the case for the nuclear quadrupole interaction (NQI) of probe nuclei in pure non-cubic metals, which has been studied extensively, very little information has been collected for the case of NQIs in ordered intermetallic compounds. In comparison with pure metals, intermetallic compounds offer more features for investigation by the probe ion within the same lattice, such as a variety of well defined crystallographic surroundings consisting of different atoms positioned at different interatomic distances, as well as the opportunity to establish the degree of order and the nature of the phase transition in the lattice. Hence, this large group of compounds opens up new possibilities for investigation

0953-8984/98/286285+15$19.50  

of parameters which characterize the metallic state and contribute to a better understanding of the properties of EFGs in metals.

In recent years, very sophisticated and precise TDPAC gamma-ray spectroscopy has been used for the investigation of the nuclear quadrupole interaction of probe nuclei in non-cubic intermetallic compounds of the transition metal Hf [1, 2]. In TDPAC experiments, probe atoms are introduced into the material in trace amounts, and they interact with electric and/or magnetic fields in their vicinity, which are produced by the surrounding atoms, ions, and electrons. As suitable TDPAC probes have an excited nuclear state, hyperfine interactions are traced via the gamma–gamma cascade of the probe radioactive decay. A start gamma ray signals the creation of the intermediate state and a stop gamma ray indicates when the state has decayed. The anisotropic intensity distribution of the second $\gamma$-quantum with respect to the direction of propagation of the first one is known as the angular correlation of the two nuclear radiations. All physical information concerning the perturbation of the angular correlation by extranuclear fields is expressed through some perturbation factor which mainly depends on the principal component of the EFG tensor and the asymmetry parameter $\eta$. If an intermediate state of a suitable TDPAC probe lives long enough for the nuclear spin to precess through an appreciable angle during the intermediate-state lifetime, then coupling frequencies can be measured with good precision, better than 1%. The most favourable probes are $^{111}$In decaying into $^{111}$Cd, and $^{181}$Hf decaying into $^{181}$Ta, so Hf intermetallic compounds are very suitable for hyperfine-field measurements by means of the TDPAC experimental technique.

The EFG is a ground-state property of a solid, and depends sensitively on the asymmetry of the electronic charge in a crystal. In complex materials the EFG is ideally suited for the purpose of obtaining a detailed charge distribution. A theoretical understanding of the origin of the EFG has now been successfully achieved, mainly due to the work of Blaha and collaborators [9]. Their theory is based on the *ab initio* full-potential (FP) linearized-augmented-plane-wave (LAPW) method for self-consistent electronic structure calculations. In the LAPW method the wavefunctions are expressed in terms of atomic-like functions and plane waves (in the interstitial region beyond the non-overlapping muffin-tin spheres around the atoms). This method is very onerous computationally for compounds with many atoms per primitive cell.

Because of this, several groups tried to develop schemes for EFG calculation which are intermediate between full-blown expensive LAPW calculations and simple unrealistic models based on the point-charge model with empirical Sternheimer shielding and antishielding factors [10]. For a brief review of the different attempts to calculate the EFG, we refer the reader to our recent work [11]. There, we suggested using a FP LMTO ASA method developed by Savrasov and Savrasov [12] for the calculation of the EFGs in complex compounds. This method takes into account non-spherical terms in the charge density, as well as in the potential, and a multiple-$\kappa$ LMTO basis, and this is all within the ASA approximation. It permits easy, fast, and precise band calculations to be carried out for compounds with many atoms per primitive cell, for which other full-potential methods are extremely time consuming. According to the investigations performed in [11], the FP LMTO ASA method of Savrasov and Savrasov is probably the best choice currently available for the calculation of the EFGs of complex compounds.

In order to check our conclusions as regards the appropriateness of the FP LMTO ASA method for EFG calculations, we intend to present here investigations of $Hf_2Ni$ in the C16-type crystal structure with six atoms per primitive cell. Our treatment of this compound has been motivated by the existence of very precise TDPAC EFG measurements with an oversimplified theoretical explanation of the different contributions to the EFG

published recently [2].

The layout of the present paper is as follows. Firstly, in section 2, we describe the details of the fully self-consistent paramagnetic calculations specific to the $Hf_2Ni$ compound. In section 3 we present formulae for all of the components of the EFG tensor in an arbitrary coordinate system, and the evaluation of the EFG tensor at Hf and Ni sites, together with the asymmetry parameter $\eta$ for Hf, and briefly discuss the origin of the EFGs at Hf and Ni sites. In the conclusion of the paper, we discuss the agreement of our theoretical results and the TDPAC measurements for $Hf_2Ni$ presented in reference [2]. The appendix presents the detailed derivation of all of the components of the EFG tensor. To the best of our knowledge, this is the first fully detailed derivation for the case in which overlapping atomic spheres (ASA) fill all of the space of a crystal.

## 2. Details of the band-structure calculations

The self-consistent paramagnetic electronic structure calculations were carried out for the intermetallic compound $Hf_2Ni$. Its bands were calculated by the use of the first-principles version of the FP LMTO ASA method [12]. This is a simpler version of the complete FP LMTO method [13], in which are taken into account non-muffin-tin (MT) corrections using the angular momentum representation for all relevant quantities within the MT spheres, as well as in the interstitial region. The FP LMTO ASA takes into account non-spherical terms in the charge density, as well as in the potential, and a multiple-$\kappa$ LMTO basis ($\kappa^2$ is the energy of the electronic orbital outside the MT sphere), and this is all within the atomic sphere approximation, i.e. without considering an interstitial region.

The FP LMTO ASA method is based on density-functional theory in its local-density approximation (LDA). In this formalism, the crystal space is filled with overlapping Wigner–Seitz (WS) spheres centred at each atomic position, such that the total volume of WS spheres equals the volume of the crystal. Within the spheres, the electronic wavefunction is given as a linear combination of numerical solutions of the Schrödinger equation. This equation is solved without using any shape approximation—neither for the crystal potential, nor for the electronic charge density. Due to the finite overlap of the atomic spheres, and the lack of an interstitial region in the ASA approximation, the non-spherical potential and charge density are not as accurate as those in generic full-potential methods. The FP LMTO ASA provides reasonably good bands, but it is not sufficiently accurate for calculating the phonons and distortions [12]. The electronic charge density is expressed as an angular momentum expansion inside each WS sphere:

$$\rho^{el}(\boldsymbol{r}) = \sum_{L} \rho_L(r) \mathrm{i}^l Y_L(\hat{\boldsymbol{r}}) \tag{1}$$

where $L = \{l, m\}$ and the $Y_L$ are spherical harmonics.

The advantage of the FP LMTO ASA method lies in its computational efficiency. The corresponding numerical program is very fast (nearly standard LMTO ASA speed). Its accuracy is quite sufficient for the precise calculation of the EFG [11]. Its speed and accuracy recommend this method for EFG calculations of the complex compounds with many different atoms per primitive cell, for which the use of other full-potential band calculational methods would be very time consuming.

The crystal structure of $Hf_2Ni$ is of the C16 type (typified by $CuAl_2$), with space group symmetry $D_{4h}^{18}$–$I4/mcm$ [14]. This structure is characterized by two sets of mutually orthogonal planes with a dense packing of hexagons (honeycomb structure), with Hf atoms parallel to (110) and $(1\bar{1}0)$ planes. The hexagons of different types are

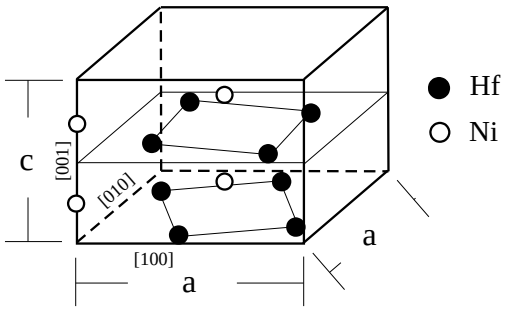


**Figure 1.** The tetragonal elementary cell for the compound $Hf_2Ni$.

fully interlocking. The Ni atoms are situated in the channels parallel to the $c$-axis, which are formed by this interlocking honeycomb structure (figure 1). A more detailed crystallographic study of binary compounds with the $CuAl_2$ C16-type structure can be found in reference [14]. The elementary cell of $Hf_2Ni$ shown in figure 1 is not the smallest one possible. This is because atoms situated in the upper half of the cell ($z \geqslant \frac{1}{2}$) can be connected with those in the lower half ($z < \frac{1}{2}$) by the same vector: $(\frac{1}{2}, \frac{1}{2}, \frac{1}{2})$. The $Hf_2Ni$ unit cell, which we used in our calculations, contains four Hf atoms at the positions $(\frac{1}{2}-u, u, 0)$, $(1-u, \frac{1}{2}-u, 0)$, $(\frac{1}{2}+u, 1-u, 0)$, $(u, \frac{1}{2}+u, 0)$, and the Ni atoms at the positions $(0, 0, \frac{1}{4})$, $(\frac{1}{2}, \frac{1}{2}, \frac{1}{4})$, where $u = 0.163$. The translational vectors are $(1, 0, 0)$, $(0, 1, 0)$, and $(\frac{1}{2}, \frac{1}{2}, \frac{1}{2})$. The $x$- and $y$-coordinates of the vectors are given in units of $a$, while the $z$-coordinate is in units of $c$. For the lattice parameters, we have used here $a = 6.479$ Å and $c = 5.271$ Å [2].

The band-structure calculation itself is characterized by the following technical details. All of the electronic states for Hf and Ni have been partitioned into the valence and core ones. The 6s, 6p, 5d, and 4f valence states were included in the basis set for Hf, and the 4s, 4p, and 3d valence states were included for Ni. The core states were considered as atomic-like (the frozen-core approximation). A one-$\kappa$ basis set has been used, with a fixed tail energy of $\kappa^2 = -0.25$ Ryd placed approximately at the centre of the occupied part of the valence panel. All of the calculations were scalar relativistic, including mass–velocity and Darwin terms, without spin–orbit interaction. The integration over $\boldsymbol{k}$-space was performed using the improved tetrahedron method [15] with a mesh of 163 points in the irreducible wedge of the first Brillouin zone. The local-density approximation of von Barth and Hedin [16] was employed in describing the exchange and correlation effects. Finally, the WS sphere radii have been chosen in such a way as to make the boundary potential values not very different for Hf and Ni, and taking into consideration the fact that the overlap between the spheres must not be too large. We found that, with the choice of 3.272 au for the Hf sphere radius and 2.671 au for the Ni sphere radius, the above-mentioned conditions were satisfied.

**Table 1.** Occupation numbers for Hf and Ni sites in the compound $Hf_2Ni$.

| | s | p | d | f | g | Charge |
|---|---|---|---|---|---|---|
| Hf | 0.754 | 0.723 | 2.602 | 13.94 | 0.053 | +0.072 |
| Ni | 0.716 | 0.602 | 8.441 | 0.058 | 0.029 | −0.144 |

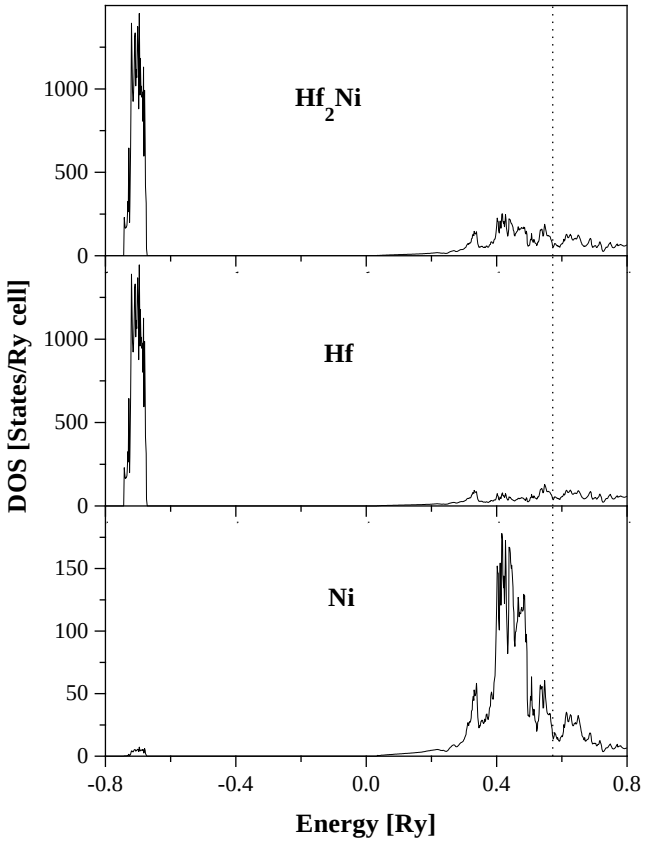


(a)

**Figure 2.** (a) The total and projected FP LMTO ASA electronic densities of states for the compound $Hf_2Ni$. The dashed line indicates the Fermi level. (b) The *l*-decomposed FP LMTO ASA electronic density of states for Hf in the compound $Hf_2Ni$. The dashed line indicates the Fermi level. (c) The *l*-decomposed FP LMTO ASA electronic density of states for Ni in the compound $Hf_2Ni$. The dashed line indicates the Fermi level.

The FP LMTO ASA electronic band structure of the intermetallic compound $Hf_2Ni$ has some notable characteristics. The main features of the electronic structure of this complex compound can be seen from the total and projected densities of states (DOS and PDOS), which are shown in figures 2(a)–2(c). These DOS curves for the paramagnetic phase exhibit the standard metallic form. The most important states around the Fermi level are hybridized d states of Hf and d states of Ni. The contributions from the s and p states of hafnium and nickel, in that region, are less significant. The calculated s and p densities of states around hafnium and nickel sites are quite similar (cf. figures 2(b) and 2(c)). The similarity of these states is reflected through the occupation numbers also. For both Hf and Ni, redistribution of atomic s electrons has occurred, filling up p and d states mostly. This can be clearly seen from table 1.

Special attention should be given to Hf f states. From figures 2(a) and 2(b) it is obvious that these states are situated far below the Fermi level, forming a very narrow zone, and retaining almost all of their own electrons (table 1). These characteristics qualify them to be considered as pure core states. However, on performing band-structure calculations

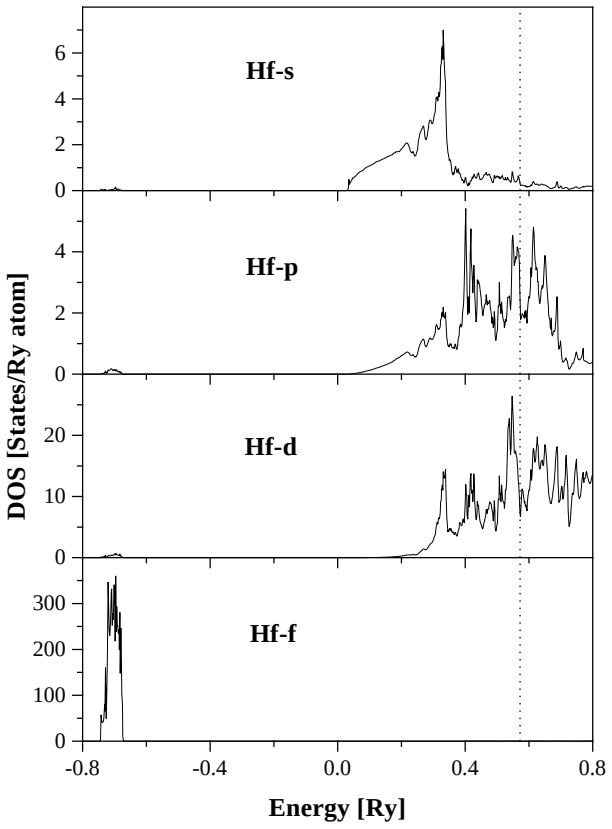


(b)

**Figure 2.** (Continued)

for $Hf_2Ni$ under the same conditions as described above, except expelling Hf 4f states from the valence basis set and putting them in the frozen core, we found some significant changes in the electronic structure. The DOS pictures look very similar to figures 2(a)–2(c) (except slight discrepancies in the Hf d zone), but the occupation numbers differ from those in table 1. This is especially so for Hf sites, where the d zone contains about 0.5 electrons fewer; these electrons are redistributed over other zones. For Ni sites, changes in the occupation numbers also occur, but they are much less pronounced. These effects do not change the electronic band picture of the compound substantially. However, they are important in EFG calculations, which will be discussed in the next section.

## 3. EFG calculations

The EFG tensor is defined as the second derivative of the electrostatic potential:

$$V_{ij} = \left.\frac{\partial^2 \Phi}{\partial x_i \, \partial x_j}\right|_{r=0} \qquad \{x_i = x, y, z\} \tag{2}$$

evaluated at the position of the nucleus. Here $V_{ij}$ is a symmetric, second-rank tensor with zero trace because of Laplace's equation $\Delta\Phi = 0$. Consequently, this tensor has only five independent components, and it can be diagonalized by rotating the coordinate system. The

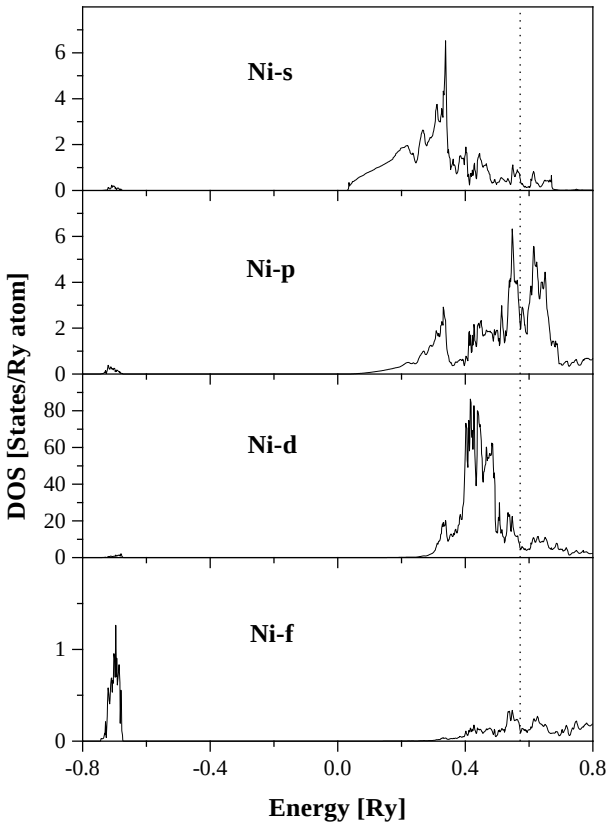


(c)

**Figure 2.** (Continued)

new coordinate system, whose principal axes are $\{X, Y, Z\}$, is usually chosen in such a way that $|V_{XX}| \leqslant |V_{YY}| \leqslant |V_{ZZ}|$. The EFG tensor is then completely determined by its principal component $V_{ZZ}$, the asymmetry parameter

$$\eta = \left| \frac{V_{XX} - V_{YY}}{V_{ZZ}} \right| \tag{3}$$

and the orientation of the principal-axis system. Finally, we should mention the existence of two special cases. For a nucleus in a cubic environment, all of the components of the EFG tensor are zero, and for one in an axially symmetrical environment holds, $\eta = 0$, i.e. $V_{XX} = V_{YY}$.

It is a common practice in the literature to separate calculations of EFGs into calculations of the valence electron contributions $V_{ij}^{val}$ and the lattice contributions $V_{ij}^{latt}$. If we write the potential $\Phi$ as a sum:

$$\Phi = \Phi^{ins} + \Phi^{out} \tag{4}$$

where $\Phi^{ins}$ is the potential generated by the charge density inside the observed atomic

sphere, while $\Phi^{out}$ is determined by the charge density from the rest of the crystal, then

$$V_{ij}^{val} = \left.\frac{\partial^2 \Phi^{ins}}{\partial x_i \, \partial x_j}\right|_{r=0}$$
$$V_{ij}^{latt} = \left.\frac{\partial^2 \Phi^{out}}{\partial x_i \, \partial x_j}\right|_{r=0}. \tag{5}$$

Here, we should note that the above separation of the EFG tensor is exact only if one is dealing with elemental metals. This is because the EFG depends on the choice of the atomic sphere radii. The way in which the crystal is subdivided into spheres is fixed for elemental metals. All atomic spheres should have equal radii, and the total volume of the spheres must be equal to the volume of the crystal. For compounds, however, there is more than one choice for the sphere radii. Thus, separation (5) makes sense only if $V_{ij}^{val}$ and $V_{ij}^{latt}$ change very slowly upon variation of the atomic sphere radii. For the case of $Hf_2Ni$, this condition is satisfied.

All of the details concerning the calculations of $V_{ij}^{val}$ and $V_{ij}^{latt}$ on the basis of equations (5) are presented in the appendix. There, we have given formulae for all of the components of the EFG tensor, in an arbitrary coordinate system. These components are expressed as functions of radial charge-density coefficients $\rho_L$, the atomic sphere radii, and the quantity $Q_L$, for whose evaluation only the matrix of structure constants and the charge multipole moments are needed (see (A14); in this section we have omitted the atomic index $\tau$). These are the quantities usually needed in the course of electronic structure calculations. In this way, only minor modifications of existing computer codes for the band-structure calculations are necessary in order to obtain the EFG tensor.

After accomplishing self-consistency for the electronic structure under the conditions described in previous section, we have evaluated the EFG tensors at Hf and Ni sites in $Hf_2Ni$, by using formulae (A19) and (A20). We obtained the following results.

First of all, it turns out that the lattice contribution to the EFG tensor is negligible, about 1% for both Hf and Ni sites. This result is often obtained in EFG calculations for close-packed metals, and could be explained by the efficiency of the charge screening in these systems. This is confirmed by the very small charge transfer from Ni to Hf WS spheres (see table 1). Consequently, from now on we can consider the total EFG to consist of valence electron contributions only.

For Hf sites, besides diagonal components, there exists a large $V_{xy}$-component of the EFG tensor (in the coordinate system indicated in figure 1). After carrying out the transformation to the principal-axis system, we obtained only diagonal components: $V_{XX} = +2.0$, $V_{YY} = +6.9$, and for the main component we obtained $V_{ZZ} = -8.9$, in units of $10^{17}$ V cm$^{-2}$. The value of the asymmetry parameter obtained in this way is $\eta = 0.556$. The experimental value for the main component of the EFG tensor is $V_{ZZ} = 10.5$, in units of $10^{17}$ V cm$^{-2}$ (the sign is undetermined), while the asymmetry parameter is $\eta = 0.744$ [2]. The time-differential perturbed angular correlation (TDPAC) measurements were performed at a temperature of 78 K, and the EFG was determined using the value of the quadrupole moment of $Q = +2.36 \times 10^{-24}$ cm$^2$ from reference [17].

The theoretical value for the $V_{ZZ}$-component at the Hf site is 15% smaller than the corresponding experimental value, while the asymmetry parameter has a value about 25% smaller than the experimental one. Taking into account the fact that the EFG is a very subtle quantity, as well as the fact that the experiment was performed on polycrystalline samples, we could say that the agreement between our theoretical results and the experimental data is quite acceptable.

As regards the orientation of the EFG tensor, our calculations predict that $V_{XX}$ points in the [001] direction, $V_{YY}$ in the $[\bar{1}10]$ direction, while $V_{ZZ}$ is parallel to the [110] direction. This holds for the Hf sites at the positions $(\frac{1}{2}-u, u, 0)$ and $(\frac{1}{2}+u, 1-u, 0)$. For the Hf sites at the positions $(1-u, \frac{1}{2}-u, 0)$ and $(u, \frac{1}{2}+u, 0)$, we have a different situation. $V_{XX}$ still points in the [001] direction, but $V_{YY}$ is parallel to the [110] direction, while $V_{ZZ}$ is parallel to the $[\bar{1}10]$ direction.

Ni atoms are located at sites which have an axial symmetry (the $c$-axis is the crystalline symmetry axis). Therefore, the EFG tensor is diagonal, with the asymmetry parameter $\eta = 0$. For the main component of the EFG tensor we obtained $V_{ZZ} = +0.7 \times 10^{17}$ V cm$^{-2}$ (pointing in the direction parallel to the $c$-axis). There are no experimental data available for Ni sites in $Hf_2Ni$.

Next, a few words should be said about the origin of the EFG at Hf and Ni sites. The coefficients $\rho_L(r)$, which enter the integrals (A19) for the evaluation of $V_{ij}^{val}$, can be obtained from the radial wavefunctions $\Psi_L^{j\boldsymbol{k}}(r)$ through the expansion

$$\rho_L(r) = \sum_{j,\boldsymbol{k}} \sum_{L'} \sum_{L''} \Psi_{L'}^{j\boldsymbol{k}}(r)\Psi_{L''}^{j\boldsymbol{k}}(r) G_{ll'l''}^{mm'm''} \Theta(E_F - E_{j\boldsymbol{k}}) \tag{6}$$

where $j$ denotes the band index, $G_{ll'l''}^{mm'm''}$ are Gaunt numbers, $E_F$ is the Fermi energy, and $\Theta$ is a step function. Expansion (6) enables us to establish individual contributions to the EFG from s, p, d or f electrons. On the basis of this expression, we decomposed the main components of the EFG tensor for both Hf and Ni sites, and we present them in table 2.

**Table 2.** The decomposition of the calculated $V_{ZZ}$-values in units of $10^{17}$ V cm$^{-2}$.

| | s–d | p–p | d–d | p–f | f–f | $V_{ZZ}$ |
|---|---|---|---|---|---|---|
| Hf | 0.0 | −10.1 | 1.3 | 0.0 | −0.1 | −8.9 |
| Ni | 0.0 | −1.9 | 2.6 | 0.0 | 0.0 | 0.7 |

As can be seen, the significant contributions to the EFG come from just p and d electrons, for both Hf and Ni. The contribution from the p electrons is an order of magnitude greater than the contribution from the d electrons, and dominates the EFG value for Hf sites. For Ni atoms, the two contributions are of the same order of magnitude, but with opposite signs. As a result of their cancellation, the EFG value for Ni is close to zero.

At the end, we will briefly discuss the influence on the EFG of varying the treatment of the Hf 4f electrons in band-structure calculations. Towards that aim, we have performed three different kinds of fully self-consistent FP LMTO ASA calculation, as well as corresponding EFG calculations, and compared their results.

(a) *The Hf 4f states were put in the valence panel.* This was the most accurate calculation. The f states of Hf were in the basis set, in the same energy panel as the other valence states, interacting freely with them. The calculated electronic structure and EFG have already been presented as a central feature of this paper.

(b) *The Hf 4f states were put in the semicore panel.* In this calculation, the f states of Hf were treated in the same way as the valence states (in a self-consistent manner), but in a separate energy window. The electronic structure obtained is similar to that derived in procedure (a). As regards the EFG, for the Hf sites we obtained $V_{ZZ} = -10.6 \times 10^{17}$ V cm$^{-2}$, almost reaching the experimental value. A slightly worse agreement with experiment was found for the asymmetry parameter: $\eta = 0.477$. The decomposition of $V_{ZZ}$ is quite similar

to that in (a). For Ni sites, the value of $V_{ZZ}$ found was identical to that obtained from procedure (a).

(c) *The Hf 4f states were put in the frozen deep core.* This was the least accurate calculation. The 4f states of Hf were considered as atomic-like, with no interaction with the valence states. The electronic structure obtained was briefly discussed in the previous section. For the main component of the EFG tensor at Hf sites we obtained $V_{ZZ} = -18.0 \times 10^{17}$ V cm$^{-2}$, which is twice the value obtained using procedure (a). For the asymmetry parameter, $\eta = 0.474$ was obtained. Decomposition of $V_{ZZ}$ gave $-17.9$ and $+2.2$ from the p and d electrons respectively, but also an unusually large contribution from the valence f electrons: $-2.3$, which almost cancelled the d contribution. In the case of Ni atoms, $V_{ZZ}$ even changed the sign. We obtained $V_{ZZ} = -1.1 \times 10^{17}$ V cm$^{-2}$, as a consequence of the fact that the p-electron contribution ($-3.3$) became larger than the d-electron contribution ($+2.2$).

From the above considerations, it is clear that Hf 4f electrons play an important role in the determination of the EFG tensor in the compound $Hf_2Ni$. Their influence on the EFG values for both Hf and Ni atoms is not manifested directly, through the p–f and f–f contributions, which are almost zero (table 2). However, interaction of Hf 4f electrons with other valence states in the compound changes electronic distribution and occupation numbers of the latter. Owing to this, contributions to the EFG from other valence states are changed also. This is especially so for the p and d states of Hf and Ni, whose contributions as obtained from procedures (a) and (c) differ significantly. On the basis of these facts, we concluded that the 4f states of Hf have to be treated in a self-consistent manner (either in the valence panel or in the semicore panel) in order for acceptable agreement with experimental data to be achieved.

## 4. Concluding remarks

The electronic structure, electric field gradient, and the corresponding asymmetry parameter $\eta$ for the intermetallic compound $Hf_2Ni$ in the single BCT C16-type structure have been calculated by the FP LMTO ASA method. Our calculations have given results for the electric field gradient and the asymmetry parameter $\eta$ that are nicely represented within the limitations of the LDA. We have obtained the electric field gradient at the Hf sites as $V_{ZZ} = -8.9 \times 10^{17}$ V cm$^{-2}$ and the asymmetry parameter $\eta = 0.556$, to be compared with the TDPAC experimentally measured values: $V_{ZZ} = 10.5 \times 10^{17}$ V cm$^{-2}$ (with the sign undefined) and $\eta = 0.744$ [2]. The importance of taking into account non-spherical terms in the charge density and potential, as well as that of the proper treatment of the Hf 4f electrons, follow from these calculations.

In order to explain the high-quality experimental data obtained for $Hf_2Ni$, the authors of reference [2] used the traditional theoretical model [3] for the decomposition of various contributions to the EFG $V_{ZZ}$ at an impurity nuclear site in a host non-cubic conducting material. The ionic contribution to the EFG was obtained by calculating two separate lattice sums with a special choice of the average number of valence electrons per atom and by the use of special empirical multiplicative Sternheimer enhancement factors (for more details, see reference [2]). They obtained $V_{ZZ}^{ion} = -18.8 \times 10^{17}$ V cm$^{-2}$ at 295 K. The corresponding asymmetry parameter is about $\eta = 0.47$. Although one should not place too much reliance on numerical values of the point-charge-model derived EFG and $\eta$, in view of the lack of exact knowledge of the ionic charges involved, the electronic contribution was calculated by simple deduction of the ionic contribution from the experimental result for the EFG.

Obviously, it is impossible to understand fully the origin of the observed behaviour of the EFG on the basis of such an oversimplified theoretical procedure, especially for metallic systems. As one might expect, the ionic contribution to the EFG obtained in reference [2] is in complete disagreement with our findings.

In concluding this work, we should say that the FP LMTO ASA method with spdf wavefunctions gives values of the EFG and $\eta$ that agree very well with experimental data. Bearing in mind the subtlety of the measured quantities, we should be very satisfied with the agreement obtained between our theoretical and experimental results. This agreement is so good and the method so fast that we can say that the FP LMTO ASA is probably the optimal choice balancing accuracy and efficiency for the EFG calculations. Differences of much greater order between the best theoretical and experimental results were observed even for several HCP metals [9, 11], where the measurements were carried out on samples of high purity. In the case of $Hf_2Ni$, the polycrystalline samples used in the TDPAC measurements of EFG and $\eta$ were synthesized from Hf with 3N purity which contains a significant level of zirconium impurities (up to 2%).

## Acknowledgment

This work was supported by the Serbian Scientific Foundation under the project 'Physics of Condensed Matter and New Materials', Grant No 3.

## Appendix

Our aim here is to evaluate all of the components of the EFG tensor on the basis of equations (5). As a first step, we have to calculate the potentials $\Phi^{ins}$ and $\Phi^{out}$.

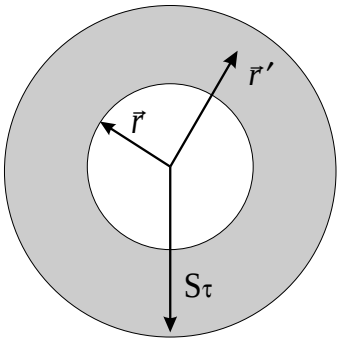


**Figure A1.** A single atomic sphere $\tau$. The charge distribution located in the shaded area generates the potential $\Phi_\tau^{ins}$ at some point $\boldsymbol{r}$.

Let us consider a single atomic sphere $\tau$ (figure A1). The potential $\Phi^{ins}$ at some point $\boldsymbol{r}$, which is generated by the charge density from the shaded area, is given by the well known formula

$$\Phi_\tau^{ins}(\boldsymbol{r}) = -\frac{|e|}{4\pi\varepsilon_0}\int \frac{\rho^{el}(\boldsymbol{r}')\ \mathrm{d}\boldsymbol{r}'}{|\boldsymbol{r}-\boldsymbol{r}'|}. \tag{A1}$$

Substituting the angular momentum expansion of $\rho^{el}(\boldsymbol{r})$, equation (1), into equation (A1), and using the spherical harmonics expansion of $1/|\boldsymbol{r}-\boldsymbol{r}'|$, after integration over

angles we finally get

$$\Phi_{\tau}^{ins}(\boldsymbol{r}) = -\frac{|e|}{4\pi\varepsilon_0}\sum_{L} r^l \mathrm{i}^l Y_L(\hat{\boldsymbol{r}})\frac{4\pi}{2l+1}\int_{r}^{S_\tau} r'^{-l-1}\rho_L(r')r'^2\,\mathrm{d}r'. \tag{A2}$$

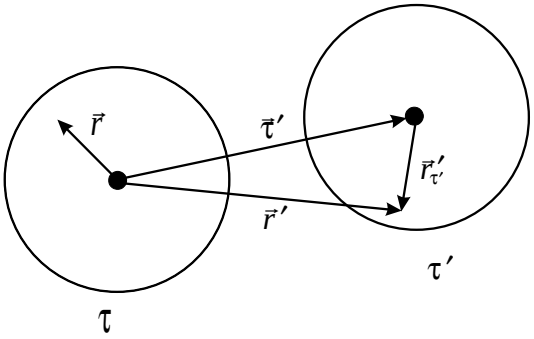


**Figure A2.** Atomic spheres $\tau$ and $\tau'$. The charge-density distribution in sphere $\tau'$ generates the potential $\Phi^{out}_{\tau\leftarrow\tau'}$ at some point $\boldsymbol{r}$ in the sphere $\tau$.

Calculation of $\Phi^{out}$ is much more complex. Let us consider a single atomic sphere $\tau$ again, and evaluate the potential $\Phi^{out}_{\tau\leftarrow\tau'}$ in that sphere, generated by the charge-density distribution located in another atomic sphere $\tau'$ (figure A2):

$$\Phi^{out}_{\tau\leftarrow\tau'}(\boldsymbol{r}) = -\frac{|e|}{4\pi\varepsilon_0}\int_{V_{\tau'}}\frac{\rho_{\tau'}(\boldsymbol{r}'_{\tau'})\,\mathrm{d}\boldsymbol{r}'}{|\boldsymbol{r}-\boldsymbol{r}'|}. \tag{A3}$$

The integration is performed over the volume of the sphere $\tau'$. If we use the notation $\boldsymbol{r}_{\tau'} = \boldsymbol{r} - \boldsymbol{\tau}'$, we can rearrange the denominator in equation (A3): $\boldsymbol{r}-\boldsymbol{r}' = \boldsymbol{r}-\boldsymbol{\tau}'-\boldsymbol{r}'_{\tau'} = \boldsymbol{r}_{\tau'}-\boldsymbol{r}'_{\tau'}$. On applying the spherical harmonic expansion of $1/(|\boldsymbol{r}_{\tau'}-\boldsymbol{r}'_{\tau'}|)$, the following expression is obtained:

$$\Phi^{out}_{\tau\leftarrow\tau'}(\boldsymbol{r}) = -\frac{|e|}{4\pi\varepsilon_0}\int_{V_{\tau'}}\rho_{\tau'}(\boldsymbol{r}'_{\tau'})\,\mathrm{d}\boldsymbol{r}'_{\tau'}\sum_{L'}\frac{4\pi}{2l'+1}\,\frac{r'^{l'}_{\tau'}}{r^{l'+1}_{\tau'}}Y^*_{L'}(\hat{\boldsymbol{r}}'_{\tau'})Y_{L'}(\hat{\boldsymbol{r}}_{\tau'}). \tag{A4}$$

It is our intention further to express $\Phi^{out}$ through the matrix of structure constants. First of all, we shall give the definitions of Bessel and Hankel functions, as well as their asymptotic behaviours when $\kappa \to 0$ that are used in our computer code:

$$J_{l\kappa\tau}(r) = \frac{(2l+1)!!}{(\kappa S_\tau)^l}j_l(\kappa r) \xrightarrow{\kappa\to 0} \left(\frac{r}{S_\tau}\right)^l \tag{A5}$$

$$H_{l\kappa\tau}(r) = -\frac{(\kappa S_\tau)^{l+1}}{(2l-1)!!}h_l(\kappa r) \xrightarrow{\kappa\to 0} \left(\frac{S_\tau}{r}\right)^{l+1} \tag{A6}$$

where $j_l$ and $h_l$ are spherical Bessel and Hankel functions respectively. The Hankel function $H$ centred at site $\tau'$ could be expanded around the site $\tau$ in terms of Bessel functions $J$, giving

$$H_{L'\kappa\tau'}(\boldsymbol{r}_{\tau'}) = -\sum_{L}\frac{1}{S_\tau(2l+1)}J_{L\kappa\tau}(\boldsymbol{r}_\tau)S_{\tau L;\tau' L'}(\kappa) \tag{A7}$$

where $H_{L'\kappa\tau'}(\boldsymbol{r}_{\tau'}) = H_{l'\kappa\tau'}(r_{\tau'})\mathrm{i}^{l'}Y_{L'}(\hat{\boldsymbol{r}}_{\tau'})$ and $J_{L\kappa\tau}(\boldsymbol{r}_\tau) = J_{l\kappa\tau}(r_\tau)\mathrm{i}^l Y_L(\hat{\boldsymbol{r}}_\tau)$. The expansion coefficients $S_{\tau L;\tau' L'}(\kappa)$ are the structure constants. In the limit $\kappa \to 0$, equation (A7)

becomes

$$\left(\frac{S_{\tau'}}{r_{\tau'}}\right)^{l'+1} \mathrm{i}^{l'} Y_{L'}(\hat{\boldsymbol{r}}_{\tau'}) = -\sum_{L} \frac{1}{S_\tau(2l+1)} \left(\frac{r_\tau}{S_\tau}\right)^{l} \mathrm{i}^{l} Y_L(r_\tau) S_{\tau L;\tau' L'}(\kappa = 0). \tag{A8}$$

Substituting the term $[1/(r_{\tau'}^{l'+1})]Y_{L'}(\hat{\boldsymbol{r}}_{\tau'})$ from equation (A8) into equation (A4), after some algebra we get

$$\Phi^{out}_{\tau \leftarrow \tau'}(\boldsymbol{r}) = \frac{|e|}{4\pi\varepsilon_0} \sum_{L} \left(\frac{r_\tau}{S_\tau}\right)^{l} \mathrm{i}^{l} Y_L(r_\tau) \frac{\sqrt{4\pi}}{S_\tau(2l+1)} \sum_{L'} S_{\tau L;\tau' L'}(\kappa = 0) \frac{M^{tot}_{L'\tau'}}{S_{\tau'}(2l'+1)} \tag{A9}$$

where the multiple moments from the sphere $\tau'$ are

$$M^{tot}_{L'\tau'} = \frac{\sqrt{4\pi}}{S^{l'}_{\tau'}} \int_{V_{\tau'}} \rho_{\tau'}(\boldsymbol{r}'_{\tau'}) r'^{l'}_{\tau'} \left[\mathrm{i}^{l'} Y_{L'}(\hat{\boldsymbol{r}}'_{\tau'})\right]^* \, \mathrm{d}\boldsymbol{r}'_{\tau'}. \tag{A10}$$

With these definitions and expansions it is now possible to evaluate $\Phi^{out}(\boldsymbol{r})$ in the sphere $\tau$ by means of summing the contributions from other spheres in the elementary cell, as well as those from all other elementary cells in a crystal:

$$\Phi^{out}_{\tau}(\boldsymbol{r}) = \sum_{\boldsymbol{T} \neq \boldsymbol{\tau} - \boldsymbol{\tau}'} \sum_{\boldsymbol{\tau}'} \Phi^{out}_{\tau \leftarrow \tau' + \boldsymbol{T}}(\boldsymbol{r}) \tag{A11}$$

where $\boldsymbol{T}$ is the translational vector of the crystal lattice. Taking into account the fact that

$$\sum_{\boldsymbol{T} \neq \boldsymbol{\tau} - \boldsymbol{\tau}'} S_{\tau L;(\tau' + \boldsymbol{T}) L'}(\kappa = 0) = S^{\boldsymbol{k}=0}_{\tau L;\tau' L'}(\kappa = 0) \tag{A12}$$

we finally obtain

$$\Phi^{out}_{\tau}(\boldsymbol{r}) = -\frac{|e|}{4\pi\varepsilon_0} \sum_{L} \left(\frac{r_\tau}{S_\tau}\right)^{l} \mathrm{i}^{l} Y_L(\hat{\boldsymbol{r}}_\tau) Q_{L\tau} \tag{A13}$$

where the vector $Q_{L\tau}$ is given as

$$Q_{L\tau} = -\frac{\sqrt{4\pi}}{S_\tau(2l+1)} \sum_{L'} \sum_{\boldsymbol{\tau}'} S^{\boldsymbol{k}=0}_{\tau L;\tau' L'}(\kappa = 0) \frac{M^{tot}_{L'\tau'}}{S_{\tau'}(2l'+1)}. \tag{A14}$$

As a last step, we have to transform the expression (A10) into the more convenient form. If we now write the total charge-density function $\rho^{tot}_{\tau'}$ as a sum of two contributions:

$$\rho_{\tau'}(\boldsymbol{r}'_{\tau'}) = -z_{\tau'} \delta(\boldsymbol{r}'_{\tau'}) + \rho^{el}_{\tau'}(\boldsymbol{r}'_{\tau'}) \tag{A15}$$

and substitute this expression into (A10), we find

$$M^{tot}_{L'\tau'} = -z_{\tau'} \delta_{L'0} + \frac{\sqrt{4\pi}}{S^{l'}_{\tau'}} \int_0^{S_{\tau'}} r'^{l'}_{\tau'} \rho_{L'\tau'}(r'_{\tau'}) r'^{2}_{\tau'} \, \mathrm{d}r'_{\tau'}. \tag{A16}$$

The first term in the expression (A15) is the contribution to the density from the point charge of the nucleus, while the second term is the electronic charge density (both from atomic sphere $\tau'$).

The formula for the electrostatic potential in the chosen sphere $\tau$, equation (A13), displays the contribution from all charges outside the sphere. This potential depends on the coefficients $\rho_{L\tau}$ and the matrix of structure constants $S$ for $\boldsymbol{k} = 0$ and $\kappa = 0$. These quantities were obtained from the FP LMTO ASA computer code after self-consistency was achieved.

Finally, we wish to evaluate the components of the EFG tensor, on the basis of equations (5). To do this we need the derivatives of the function $r^l Y_L(\hat{\boldsymbol{r}})$. In order to solve this problem, we have used the expressions

$$\begin{aligned}
\nabla_0[f(r)Y_l^m(\hat{\boldsymbol{r}})] &= \sqrt{\frac{(l+1)^2-m^2}{(2l+1)(2l+3)}}\left(\frac{\mathrm{d}f}{\mathrm{d}r}-\frac{l}{r}f\right)Y_{l+1}^m \\
&\quad+\sqrt{\frac{l^2-m^2}{(2l-1)(2l+1)}}\left(\frac{\mathrm{d}f}{\mathrm{d}r}+\frac{l+1}{r}f\right)Y_{l-1}^m \\
\nabla_{\pm1}[f(r)Y_l^m(\hat{\boldsymbol{r}})] &= \sqrt{\frac{(l\pm m+1)(l\pm m+2)}{2(2l+1)(2l+3)}}\left(\frac{\mathrm{d}f}{\mathrm{d}r}-\frac{l}{r}f\right)Y_{l+1}^{m\pm1} \\
&\quad-\sqrt{\frac{(l\mp m-1)(l\mp m)}{2(2l-1)(2l+1)}}\left(\frac{\mathrm{d}f}{\mathrm{d}r}+\frac{l+1}{r}f\right)Y_{l-1}^{m\pm1}
\end{aligned} \tag{A17}$$

in the cyclic coordinate system [18]. Back-transformation to the Cartesian coordinate system gives for the partial derivatives

$$\begin{aligned}
\frac{\partial}{\partial x} &= -\frac{1}{\sqrt{2}}(\nabla_1-\nabla_{-1}) \\
\frac{\partial}{\partial y} &= \frac{\mathrm{i}}{\sqrt{2}}(\nabla_1+\nabla_{-1}) \\
\frac{\partial}{\partial z} &= \nabla_0.
\end{aligned} \tag{A18}$$

The EFG is now given by the sum of expressions (5), (A2), (A13), (A17), and (A18). After straightforward but tedious calculations, one can obtain the valence electron contributions:

$$\begin{aligned}
V_{xx}^{val} &= \frac{|e|}{4\pi\varepsilon_0}\sqrt{\frac{6\pi}{5}}\int_0^S \frac{\rho_{22}+\rho_{2-2}-\sqrt{\frac{2}{3}}\rho_{20}}{r}\,\mathrm{d}r \\
V_{yy}^{val} &= \frac{|e|}{4\pi\varepsilon_0}\sqrt{\frac{6\pi}{5}}\int_0^S \frac{-(\rho_{22}+\rho_{2-2})-\sqrt{\frac{2}{3}}\rho_{20}}{r}\,\mathrm{d}r \\
V_{zz}^{val} &= \frac{|e|}{4\pi\varepsilon_0}\sqrt{\frac{16\pi}{5}}\int_0^S \frac{\rho_{20}}{r}\,\mathrm{d}r \\
V_{xy}^{val} &= -\mathrm{i}\frac{|e|}{4\pi\varepsilon_0}\sqrt{\frac{6\pi}{5}}\int_0^S \frac{\rho_{2-2}-\rho_{22}}{r}\,\mathrm{d}r \\
V_{xz}^{val} &= \frac{|e|}{4\pi\varepsilon_0}\sqrt{\frac{6\pi}{5}}\int_0^S \frac{\rho_{2-1}-\rho_{21}}{r}\,\mathrm{d}r \\
V_{yz}^{val} &= -\mathrm{i}\frac{|e|}{4\pi\varepsilon_0}\sqrt{\frac{6\pi}{5}}\int_0^S \frac{\rho_{2-1}+\rho_{21}}{r}\,\mathrm{d}r
\end{aligned} \tag{A19}$$

and the lattice contributions:

$$
\begin{aligned}
V_{xx}^{latt} &= \frac{|e|}{4\pi\varepsilon_0}\sqrt{\frac{5}{4\pi}}\frac{1}{2S_\tau^2}\left[\sqrt{6}(Q_{22\tau}+Q_{2-2\tau})-2Q_{20\tau}\right] \\
V_{yy}^{latt} &= \frac{|e|}{4\pi\varepsilon_0}\sqrt{\frac{5}{4\pi}}\frac{1}{2S_\tau^2}\left[-\sqrt{6}(Q_{22\tau}+Q_{2-2\tau})-2Q_{20\tau}\right] \\
V_{zz}^{latt} &= \frac{|e|}{4\pi\varepsilon_0}\sqrt{\frac{5}{\pi}}\frac{1}{S_\tau^2}Q_{20\tau} \\
V_{xy}^{latt} &= -\mathrm{i}\frac{|e|}{4\pi\varepsilon_0}\sqrt{\frac{15}{2\pi}}\frac{1}{2S_\tau^2}(Q_{2-2\tau}-Q_{22\tau}) \\
V_{xz}^{latt} &= \frac{|e|}{4\pi\varepsilon_0}\sqrt{\frac{15}{2\pi}}\frac{1}{2S_\tau^2}(Q_{2-1\tau}-Q_{21\tau}) \\
V_{yz}^{latt} &= -\mathrm{i}\frac{|e|}{4\pi\varepsilon_0}\sqrt{\frac{15}{2\pi}}\frac{1}{2S_\tau^2}(Q_{2-1\tau}+Q_{21\tau})
\end{aligned}
\tag{A20}
$$

to the EFG tensor. These formulae are valid for all types of crystal structure, i.e. they do not depend on the symmetry. They completely determine the EFG tensor, and can be used in any band-structure calculation method which employs the ASA. In the case of non-ASA methods, the contribution to the EFG from the interstitial region has to be added.

## References


[1] Koički S, Cekić B, Ivanović N and Manasijević M 1993 *Phys. Rev.* B **48** 9291
[2] Manasijević M, Koički S, Cekić B and Ivanović N 1994 *J. Phys.: Condens. Matter* **6** 9781
[3] Kaufmann E N and Vianden R J 1979 *Rev. Mod. Phys.* **51** 161
Vianden R J, Kaufmann E N, Naumann R A and Schmidt G 1979 *Hyperfine Interact.* **7** 247
[4] Vianden R J 1983 *Hyperfine Interact.* **15+16** 189
[5] Klas T, Voigt J, Keppner W, Wesche R and Schatz G 1986 *Phys. Rev. Lett.* **57** 1068
[6] Pleiter F and Hohenemser C 1985 *Phys. Rev.* B **25** 106
[7] Wichart T R and Swanson M L 1990 *Hyperfine Interact.* **62** 231
[8] Collins G S, Shropshire S L and Fou J 1990 *Hyperfine Interact.* **62** 1
[9] Blaha P, Schwarz K and Herzig P 1985 *Phys. Rev. Lett.* **54** 1192
Blaha P and Schwarz K 1987 *J. Phys. F: Met. Phys.* **17** 899
Blaha P, Schwarz K and Dederichs P H 1988 *Phys. Rev.* B **37** 2792
[10] Cjzek G, Jink J, Gotz F, Schmidt H, Coey J M D, Rebooillat J P and Lienard A 1981 *Phys. Rev.* B **23** 2513
[11] Lalić M V, Popović Z S and Vukajlović F R 1998 *Physica* B **245** 376
[12] Savrasov S Yu and Savrasov D Yu 1996 *Full Potential LMTO Program User's Manual* unpublished
[13] Savrasov S Yu and Savrasov D Yu 1992 *Phys. Rev.* B **46** 12 181
[14] Havinga E E, Damsma H and Hokkeling P 1972 *J. Less-Common Met.* **27** 169
[15] Blöchl P E, Jepsen O and Andersen O K 1994 *Phys. Rev.* B **49** 16 223
[16] von Barth U and Hedin L 1972 *J. Phys. C: Solid State Phys.* **5** 1629
[17] Butz T and Lerf A 1983 *Phys. Lett.* **97A** 217
[18] Varshalovich D A, Moskalev A N and Khersonskii V K 1988 *Quantum Theory of Angular Momentum* (Singapore: World Scientific)